polymers

MDPI

Article

Cyclodextrins and their polymers affect the lipid membrane permeability and increase levofloxacin's antibacterial activity *in vitro*

Anna A. Skuredina [1], Anastasia S. Tychinina [1], Irina M. Le-Deygen [1,*], Sergey A. Golyshev [2], Tatiana Yu. Kopnova [1], Nikolay T. Le [3], Natalya G. Belogurova [1] and Elena V. Kudryashova [1,*]

[1] Chemistry Department, Lomonosov MSU, 119991 Moscow, Russia; skuredinanna@gmail.com (A.A.S.); tychinina.a@yandex.ru (A.S.T.); kopnovataty@gmail.com (T. Yu.K.); nbelog@mail.ru (N.G.B.)

[2] Belozersky Institute of Physico-Chemical Biology, Lomonosov MSU, 119991, Moscow, Russia; sergei.a.golyshev@gmail.com (S.A.G.)

[3] Faculty of Physics, Lomonosov MSU, 119991 Moscow, Russia; lenickola@mail.ru (N.T.L.)

* Correspondence: i.m.deygen@gmail.com (I.M.L.-D.); helenakoudriachova@yandex.ru (E.V.K.)

Citation: Lastname, F.; Lastname, F.; Lastname, F. Title. *Polymers* **2022**, *14*, x. https://doi.org/10.3390/xxxxx

Academic Editor: Firstname Lastname

Received: date

Accepted: date

Published: date

Abstract: Cyclodextrins (CDs) are very promising drug carriers that are used in medicine. We chose CDs with different substituent (polar/apolar, charged/neutral) to obtain polymers (CDpols) with different properties. CDpols are urethanes with the average Mw ~120 kDa, they form nanoparticles 100-150 nm in diameter with variable ζ-potential. We studied CD' and CDpols' interaction with model (liposomal) and bacterial membranes. Both types of CD carriers cause the increase of the liposomal membrane permeability, and for polymers this effect is almost 2 times stronger. The formation of CD/CDpols complexes with levofloxacin (LV) enhances LV's antibacterial action 2 times *in vitro* on 5 bacterial strain. The most pronounced effect was determined for LV-CD complexes. LV-CDs and LV-CDpols adsorb on bacteria, and cells' morphology influence this process dramatically. According to TEM studies «rough» surface and proteinaceous fimbria of gram-negative *E . coli* faciliate adsorption of CD particles, whereas smooth surface of gram-positive bacteria impedes it. In comparison with LV-CDs LV-CDpols are adsorbed 15% more effectively by *E.coli*, 2.3 times better by lactobacilli and 5 times better in case of *B. subtilis*. CDs' and CDpols' are not toxic for bacterial cells, but may cause mild defects that, in addition to LV-CD carrier adsorbtion, improve LV's antibacterial properties.

Keywords: cyclodextrin; levofloxacin; liposome; spectroscopy; antibacterial activity;

1. Introduction

A large number of infectious diseases require complex, long-term medication regimens. Due to the low efficacy and poor bioavailability of some drugs, the standard course of treatment may require high dosage therapy, poteantially causing dangerous side effects [1,2]. Thus, the development of new drug formulations using drug delivery systems with increased bioavailability and safety is of great benefit to the society.

FDA approved oligosaccharides cyclodextrins (CDs) to design new drug delivery systems. CDs are low cost, possess high solubility, and can be administrated in various ways [3]. The modification of CD's hydroxyl groups by amination, alkyla-

tion, etc. widens the perspective of CDs' usage, and nowadays not the native CDs, but their derivatives, are in the spotlight [4]. CDs consist of D-glucopyranose units that form a truncated torus with a hydrophilic surface and a hydrophobic cavity. The hydrophobic cavity enables CDs to encapsulate hydrophobic drug molecules (or their fragments), forming non-covalent inclusion «guest-host» complexes. Complex formation leads to the improvement of drug's physical-chemical properties: the increase of its solubility, stability and bioavailability [5–8].

The modern trend in CDs' chemistry is the synthesis of polymers-based on CD's derivatives (CDpols) by various likers: epichlorohydrin [9,10], diisocyanate [11,12], carbonyldiimidazole [13], etc. CDpols have clear advantage: cargo molecules form a complex with the CDs torus, and, in addition, «get stuck» in a polymer's network. This makes CDpols carriers promissing as drug delivery systems with sustained drug release [12,14].

Commonly, the authors study the physical-chemical properties of drug-CD or drug-CDpol complexes [15,16], however the interaction of such systems with biological structures, for instance, membranes, remains in consideration. It is known that CDs do not penetrate through the biological barriers, but can adhere to the cell's surface [17]. Nevertheless, how one can predict CD-based carrier's interaction with membranes? Since the large number of available CDs with different substituents, it is important to determine the most promising carriers for drug delivery. Recently, we have demonstrated that CDs cause mild defects in liposomal membrane [18], but it is not clear how significant are these *in vitro* observed defects in terms of drug's antibacterial activity?

Here, we study the interaction between CD based drug carriers (CDs and CDpols) with liposomal and bacterial membranes in order to establish the effect of CD's on the antibacterial activity of drugs *in vitro* and the mechanism of such case. The purpose of this work is to establish the most promising carrier and determine the specific parameters of bacterial membrane that must be taken into account while designing the novel CD based drug delivery systems.

2. Materials and Methods

2.1 Materials

2-hydroxypropyl β-cyclodextrin (HPCD), methyl β-cyclodextrin (MCD), levofloxacin (LV), phenolphthalein (PP), Triton X-100, 1,6-hexamethylenediisocyanate, dimethyl sulfoxide (DMSO), are all from Sigma-Aldrich (USA). Sulfobutyl ether β-cyclodextrin sodium salt (SBECD) is from Zibo Qianhui Biotechnology Co. (China). Amino β-cyclodextrin (AMCD) was purchased from Shandong Binzhou Zhiyuan (China). Dipalmitoylphosphatidylcholine (DPPL) and cardiolipin (CL; 1,3-bis(sn-3'-phosphatidyl)-sn-glycerin) were purchased from Avanti Polar Lipids (USA). HCl, copper (II) sulfate, ethanol, and acetone were all purchased from Reakhim (Russian Federation). Sodium phosphate buffer tablets for solution preparation were obtained from Pan-Eco (Russian Federation). Lead citrate is from Serva (Germany). Sodium cacodylate, osmium tetroxide, and phosphor-tungstic acid were all purchased from SPI (USA).

Bacterial strains: Gram-negative bacterial strains *Escherichia coli* MH1 [19] M. Hall, USA), *E. coli* JM109 [20] (J. Messing, USA), *E. coli* ATCC 25922 and *Bacillus subtilis* ATCC 6633 (from the Russian collection of industrial microorganisms National Research Institute «Kurchatov Institute»), *Lactobacillus fermentum* 90T-C4 (from «Microgen», Russian Federation).

2.2 CDpol's synthesis

The synthesis of CDpols was performed according to [21]. Briefly, an warm aqueous solution of 5-7 mg/mL HPCD, MCD, SBECD or AMCD was mixed with DMSO for 5 min. The linker's solution (16,8 mg/mL of 1,6-hexamethelendiisocyanate in DMSO) was added dropwise upon intense stirring. The molar ratio CD derivative : linker was 1 : 3. The final solution (H_2O : DMSO ratio was 1:1 vol/vol) was exposed for 3 h at 25°C. The purification of 5 mL of each sample from organic solvent was conducted by dialysis (MWCO Serva 3.5 kDa membrane) for 24 h at 37°C with intense shaking and periodic renewal of the external solution (500-600 mL of distilled water). The aqueous solutions were frozen at −18°C for 12 h, then were stored at −70°C for 24 h and were lyophilized for 72 h at −60°C by a freeze-dryer Thermo Scientific (USA). The concentration of CD-torus in CDpols was determined by FTIR spectroscopy in accordance with the intensity of the band in the region 1050-1030 cm^{-1} that is corresponded to C-O-C bond of CDs.

2.3 Preparation of liposomes loaded with phenolphthalein

25 mg/mL of DPPC and 25 mg/mL of CL lipids (both in chloroform) were mixed to obtain a solution with DPPC : CL ratio of 80 : 20 (weight %). The removal of chloroform was conducted by evaporation at 50-55°C using a vacuum rotary evaporator. The obtained thin lipid film in glass flask was dispersed in 10^{-6} M phenolphthalein solution (0.02 M sodium phosphate buffer solution, pH 7.4). The liposomes (3 mg/ml of lipids) were sonicated at a frequency of 22 kHz three times for 200 s each using a homogenizer (4710 model, Cole-Parmer Instrument, USA) at 50–55°C. Unloaded phenolphthalein was removed by dialysis (MWCO Serva 3.5 kDa membrane) for 3 h at 25°C with intense shaking and periodic renewal of the external solution (500-600 mL 0.02 M sodium phosphate buffer solution, pH 7.4).

2.4 The release kinetics of phenolphthalein from the liposomes

2 ml of liposome solution (3 mg/ml of lipids, DPPC : CL = 80 : 20 (weight%)) loaded with phenolphthalein was transferred to an Orange Scientific dialysis bag (MWCO 3.5 kDa), which was placed in 2 ml of 0.02 M sodium borate buffer (pH 10.7). Solutions of all CDs, CDpols ($C_{CD\ torus}$ in final solution was 30 mg/mL) or Triton X-100 were added to the liposome solution by adding to the dialysis bag. The systems were stirried for 1.5 hours at 37 ° C. UV-spectra of the external solution were recorded every 10-15 minutes.

2.5 Preparation of LV-CDs and LV-CDpols complexes

CDs and CDpols were dissolved in 0.1 mM HCl pH 4.0. LV's solution in the same pH was added to CD carriers' solution to obtain molar ratio CD torus : LV = 1:1. The complexes were stirred for 1h at 37°C. To study the interaction of LV-CD or LV-CDpol with the liposomes or bacterial cells, the prepared complexes were diluted with a 0.02 M sodium phosphate buffer solution (pH 7.4) immediately before the experiment.

2.6 Nanoparticle Tracking Analysis (NTA)

NTA was performed using the Nanosight LM10-HS instrument (Nanosight Ltd., United Kingdom). The CDpols' samples were diluted by Milli-Q purified water to obtain the solutions with a ~ 10^8 particles/mL. The measurements were carried out three times for each sample, and the values are reported with standard deviations.

2.7. *Molecular weight of CDpols*

We determined CDpols' Mr by the following formula:

$$\mathrm{Mr} = \frac{[CD] \times N_A}{n} \times Mr_m$$

The number of the particles n (particles/mL) was determined by NTA [22]. Other variables are: the concentration of CD torus *[CD]* (mole/mL) in accordance with dilution, Avogadro constant N_A, and molecular weight of the repeating unit (CD and linker) Mr_m.

2.8 Dynamic light scattering (DLS)

DLS was used to determine ζ-potentials of the samples (Zetasizer Nano S «Malvern» with 4 mW He–Ne-laser, 633 nm; United Kingdom). The experiments were performed at 25°C using the correlation of the Correlator system K7032-09 «Malvern» (United Kingdom) and software «Zetasizer Software». The measurements were carried out three times for each sample, and the values are reported with standard deviations.

2.9. UV-spectroscopy

The UV-spectroscopy was conducted using Ultrospec 2100 pro instrument (Amersham Biosciences, Germany). The spectra of released phenolphthalein were recorded within a wavelength range from 400 to 650 nm in a 1 mL quartz cell (Hellma Analytics). The concentration of phenolphthalein was determined at wavelength 550 nm.

2.10. NMR spectroscopy

^{1}H NMR spectroscopy was conducted using Bruker Avance 400 spectrometer (Germany). 5-10 mg of the sample was dissolved in D_2O, and ^{1}H NMR spectra was recorded with operating frequencies of 400 MHz. Chemical shifts (δ) in ppm are reported as quoted relative to the residual signals of D_2O (4.79 ppm).

2.11 Fluorescence Spectroscopy

Emission spectra of LV were recorded using Varian Cary Eclipse fluorimeter (United States). The measurements were carried out at λ_{ex} = 289 nm within a wavelength range of 400– 550 nm. LV demonstrates the peak with the maximum at 456 nm.

2.12 The FTIR spectroscopy

FTIR spectroscopy was conducted using a Tensor 27 instrument (Bruker, Germany) that is equipped with a liquid-nitrogen-cooled MCT detector, a thermostat (Huber, United States), attenuated total reflection cell (Bruker, Germany), ZnSe single-reflection crystal. The spectra of the samples (40-50 μL) were recorded three times (70 scans each time) within a range of 3000–900 cm^{-1} at a resolution of 1 cm^{-1} at 22°C. Dry air was pumped through the system by the air compressor (Jun-Air, Germany). The background (buffer solution) was recorded in the same manner. The spectra were analyzed using the Opus 7.0 software.

2.13 Powder X-ray Diffraction (PXRD) Analysis

PXRD patterns of 5 mg of LV or its complexes with CD carriers were recorded on a Rigaku SmartLab (Japan) equipped copper X—ray anode tube. The scanning

range was 1.5–80.0° with a step size of 5° per second. X-rays were generated with settings 60 kV and 1.5 kW.

2.14 in vitro experiments using Escherichia coli, Lactobacillus fermentum and Bacillus subtilis bacterial strains

We used the overnight culture (the bacteria were cultured in Luria Bertuni (LB) liquid medium for 12 hours, expect *Lactobacillus fermentum* 90T-C4, for which De Man, Rogosa and Sharpe agar was used). The determination of minimum inhibition (MIC) concentration was performed in solid media by agar well diffusion method [23]. Briefly, 500 μL of overnight cell's culture was distributed over the surface of agar on Petri dishes. Then, 6 wells 9 mm in diameter were incised in the medium by sterile plastic pipette tip. The 50 μL of the samples (LV's concentration was 0.01 – 0.5 μg/mL for all *E. coli* strains and *B. subtilis* ATCC 6633; 20 – 100 μg/mL for *L. fermentum* 90T-C4) was put in the wells. In 20 minutes, the plates were placed into the incubator at 37 ^{O}C. After 24 h the appeared inhibition zones were analyzed. The experiments were carried out three times for each sample, and MIC values are reported with standard deviations.

For the ultrastructural studies of bacteria, the pelleted cells (900μL of the overnight culture) were fixed with 2.5% glutaraldehyde solution (100 mM sodium cacodylate) for 24 h. Then, bacterial pellets were rinsed three times for 5 min in 100 mM sodium cacodylate under slight agitation and were post-fixed with 1% OsO_4 (100 mM sodium cacodylate) for 1 h at +4°C. The fixed cells were dehydrated by increasing ethanol concentration (50%-70%-96%). The ethanol was replaced by acetone, and was followed by epoxy resin-acetone mixtures with increasing resin content. After replacing the mixture with pure resin (Spi-pon 812, SPI Supplies), the samples were exposed at +70°C for 48 h. Ultrathin sections with a nominal thickness of 80 nm were prepared using Reichert-Jung Ultracut E ultramicrotome equipped with a Diatome Ultra 45 diamond knife. The sections were mounted on the formvar-coated copper slot-grids, and post stained with lead citrate for 3 min.

For the study of bacterial surface morphology the negative staining was conducted. 15 μL of the bacterial suspension in water were placed on the frormvar-coated 200 mesh copper grids for 60-90 seconds. The drops were blotted with the filter paper. Then, 10 μL of 1% aqueous phosphotungstic acid were applied onto the grids for 20 seconds and blotted with the filter paper. Finally, the stained samples were air-dried.

For TEM micrograph of CDpols' adsorption on *B.subtilis* we preincubated 5 mg/mL HPCDpol with 0.1 M copper (II) sulfate solution for 1 h. We centrifuged the sample (Eppendorf Minispin, 10000 rpm/min, 10 min) and removed unbonded copper (II) sulfate solution. HPCDpol-Cu^{2+} was washed 3 times using Milli-Q purified water. The 900 μL of overnight *B.subtilis* were centrifuged (Eppendorf Minispin, 7000 rpm/min, 5 min) and washed 3 times with Milli-Q purified water. Then, the HPCDpol-Cu2+ was added to bacteria cells. After 20 minutes of incubation 25 μL of the sample was placed on the copper grids for 40-60 seconds. The drops were blotted with the filter paper, and the sample was dried in air.

The samples then were analyzed and imaged on JEM-1400 electron microscope (Jeol, Japan) running at 80 kV and equipped with Quemesa digital camera (OSIS, Germany).

2.13. The LV-CD and LV-CDpols adsorption on the cells

The adsorption curves were obtained using the overnight bacteria culture (~ 8×10^8 colony forming units (CFU) / mL). The 900 μL of bacteria were centrifuged

(Eppendorf Minispin, 7000 rpm/min, 5 min) and washed 3 times with sterile 0.02 M Na-phosphate buffer solution buffer (pH 7.4). The samples containing different amounts of LV-CD or LV-CDpols in sterile buffer (pH 7.4) were added to the bacteria pellets and mixed properly. After 1 hour of incubation (37^{O}C, 100rpm), the samples were centrifuged (7000 rpm/min, 5 min), and the emission spectra of supernatant was recorded.

3. Results and discussion

For in-depth study of CDs and CDpol interaction mechanisms with liposomal and cell's membranes, we chose oligosaccharides with different substituents (Figure 1): 2-hydroxypropyl-β-cyclodextrin with a polar uncharged substituent (HPCD), methyl-β-cyclodextrin with a nonpolar uncharged substituent (MCD), negatively charged sulfobutyl ether β-cyclodextrin (SBECD) and positively charged amino-β-cyclodextrin (AMCD). We selected well-known fluoroquinolone levofloxacin (LV), as a model drug molecule suitable for «guest-host» complex formation with CD [6]. LV is widely used in an antibacterial therapy of various infections, including COVID-19-associated pneumonia [24,25].

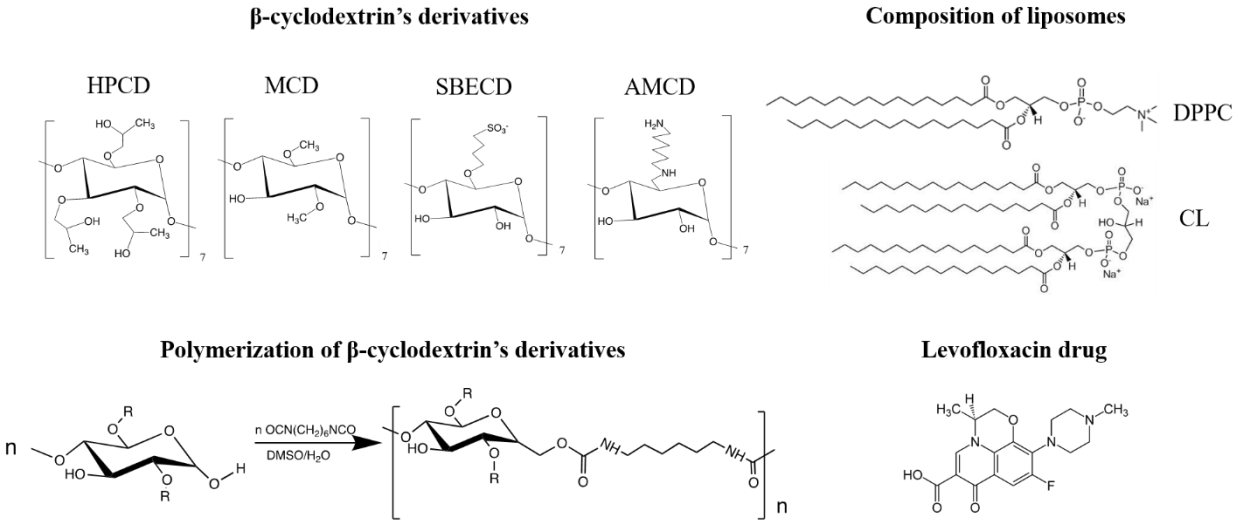

Figure 1. The structure of the β-cyclodextrin derivatives and their polymers, lipids used for liposomes production, levofloxacin.

We synthesized CDpols using 1,6-hexamethelenediisocyanate at low molar excess of crosslinking agent to obtain soluble polymers that can be used as a carriers for drug delivery.

3.1. Characterization of CDs' and CDpols' physical-chemical properties

The size, charge and the structure of CDs and CDpols might affect the interaction between the carrier and the membrane, so we studied the parameters by nanoparticle tracking analysis (NTA) and DLS (Table 1). As expected, HPCD and MCD are uncharged, while SBECD and AMCD demonstrate negative and positive ζ-potential, respectively. Thus, we are able to investigate the influence of CD's charge on its interaction with bilayer.

CD's crosslinking with 1,6-hexamethelenediisocyanate leads to formation of homogeneous nanoparticles with the average molar mass ~100−130 kDa and hydrodynamic diameter of 100-150 nm. MCDpol demonstrates the highest mass and

particle's size. Among all CDs MCD have the lowest number of available hydroxyl groups that react with cross-linking agent, so MCDpol might have linear polymeric network, whereas other CDpols − more branched polymeric network.

Table 1. The size and ζ-potential of CD, CDpol and their complexes with liposomes, pH 7.4 (0.02 M Na-phosphate buffer solution), 22°C.

	Size, nm	**ζ-potential, mV**	**Mr, kDa**	**The number of CDs per 1 particle**	**ζ-potential of liposomes + CD, mV**
HPCD	0.15 [1]	0.5 ± 0.1	1.5	−	−18.2 ± 4.4
HPCDpol	110 ± 15	9.2 ± 1.2	100 ± 15	67 ± 11	−14.3 ± 3.3
MCD	0.15 [1]	0.7 ± 0.2	1.2	−	−19.6 ± 3.4
MCDpol	165 ± 15	22.9 ± 1.2	130 ± 15	100 ± 15	−12.2 ± 2.3
SBECD	0.15 [1]	−7.7 ± 0.5	2.1	−	−24.8 ± 3.9
SBECDpol	110 ± 15	−13.4 ± 0.9	115 ± 13	65 ± 8	−14.2 ± 3.3
AMCD	0.15 [1]	6.2 ± 1.2	1.6	−	−18.5 ± 3.6
AMCDpol	122 ± 17	10.2 ± 2.2	122 ± 15	70 ± 11	−13.5 ± 2.2
Liposomes DPPC:Cl = 80:20 (weight %)	105 ± 7	−20.9±3.2	−	−	−

[1] the size of CD derivatives is assumed to be close to the size of parent CDs [26].

Interesting, that CDpols (except SBECDpol) have pronounced positive ζ-potential. This effect might be explained by spontaneous hydrolysis of 1,6-diisocyanate [27] during CDpol's synthesis and the formation of positively charged functional groups that contribute to the ζ-potential of the polymers. In case of SBECD multiple negatively charged sulfo groups might give a greater contribution that overlaps the positive charge value.

The structure of the polymers was studied by FTIR and NMR spectroscopy (Figure S1). In the ^{1}H NMR spectra of CDpols, we observed the peaks of monomer's unit and also the signals that were correlated with the methylene groups of the attached linker [28,29]. To estimate the number of attached linkers per one CD torus, the spectra were normalized by a signal corresponding to the H1 D-glucopyranose unit (doublet 5.25 ppm and 4.96 ppm): on average there are 2-3 spacers per oligosaccharide, i.e., polymers are not tightly cross-linked. It is important to note that in the concentrations required to obtain NMR spectra, CDpols do not completely dissolve in D_2O, so the obtained values may be slightly underestimated.

In CDpol's FTIR spectra we observed the appearance of 1575 cm^{-1} peak that correspond to amide bond in the urethane group. That means the synthesis performed in accordance with the scheme in Figure 1. Furthermore, the CDpol's synthesis causes the appearance of the shoulders of the absorption bands that correspond to C-O-C in glucopyranose residues (1030 – 1040 cm^{-1}). The changes in the microenvironment of C–O–C bands between glucopyranose residues in CDs derivatives after crosslinking might be the reason for that. The 951 cm^{-1} peaks determined in CDpol's spectra correspond to C-N bond in amines. Isocyanate groups hydrolysis leads to amine formation that contribute to the positive ζ-potential (Table 1).

Thus, we obtained two groups of samples that possess different size (~0,1 nm and 100-150 nm), mass (~1,2 – 2 kDa and ~120-150 kDa) and surface charge (positive, negative, neutral). These parameters might affect carrier's interaction with biological membranes.

3.2. Interaction of liposomes with CDs and CDpols

At first, we studied the effect of CD and CDpols on the integrity of model biological membrane – liposomal bilayer (DPPL/CL = 80/20 (weight %)). CDs and CDpols adsorb on liposomes that can be monitored by DLS: ζ-potential of liposome (-20 mV) slightly increases by surface charge neutralization (Table 1). The CD carrier's adsorption might lead to the changes in membrane properties.

For instance, CDs cause the defects in liposomal bilayer, but still it is not clear which CD's parameter is crucial for this effect. The occurrence of defects in the liposomal bilayer and violation of the integrity of liposomal membrane are studied by a number of authors by the analysis of the release kinetics of dyes from the vesicles [30]. We loaded anionic liposomes (DPPL/CL = 80/20 (weight %)) with indicator phenolphthalein (PP) at pH 7.4 (colorless solution). Liposomes were separated from the external solution by a dialysis membrane. The defects of liposomal membrane cause the PP's release, that can be detected in the external buffer solution with a pH of 10.7 (pink solution) at a wavelength of 550 nm (Figure 2.A).

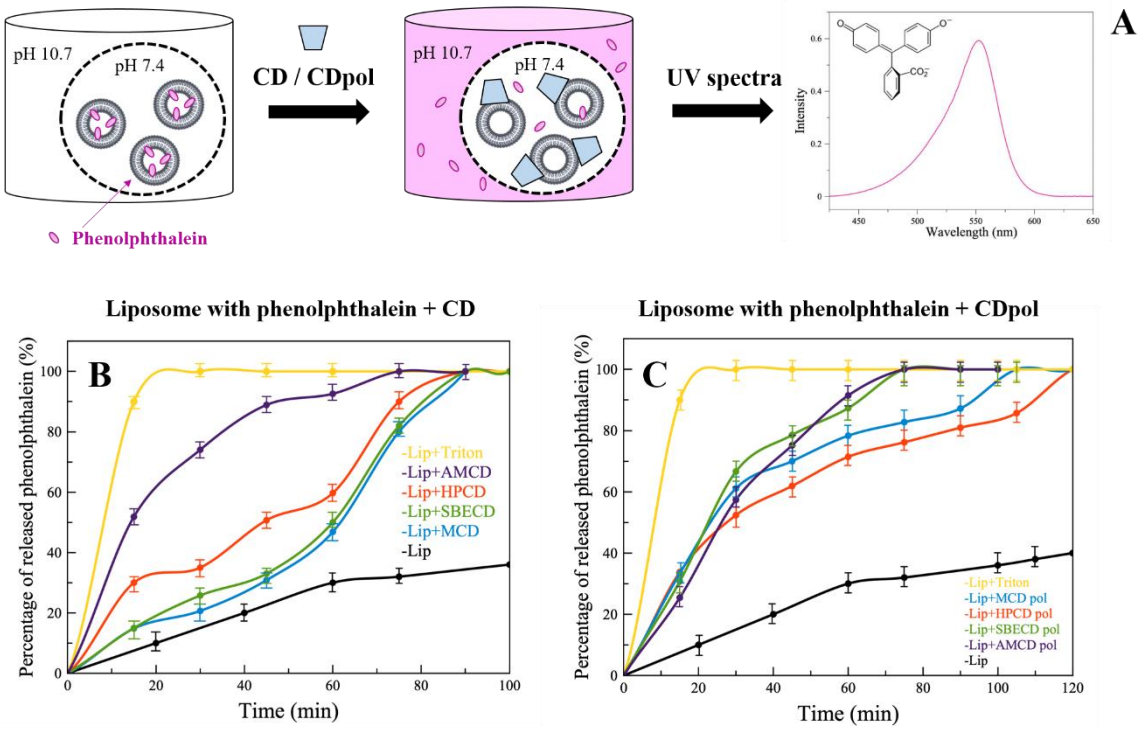

Figure 2. UV spectra of phenolphthalein (A), pH 10.7 (0.02 M Na-borate buffer solution), 22˚C**.** The release kinetics of PP from liposomes DPPC:CL = 80:20 (weight %) after adding CD (B) or CDpol (C), $C_{CD\ torus}$ = 30 mg/mL, pH 7.4 (0.02 M Na-phosphate buffer solution), pH 10.7 (0.02 M Na-borate buffer solution), 37˚C.

Control liposomes (in the absence of CD) release about 40% of PP in 120 minutes (Figure 2.B and C, black curves). For complete destruction of liposomes (100% release of PP), the well-known surfactant Triton X-100 (0.4% by weight) was added.

Triton X-100 significantly accelerates PP's release: 100% of the indicator is released after 20 minutes (Figure 2.B and C, yellow curves).

When CD's derivatives are added, a sustained PP's release is observed (Figure 2.B), compared to the control, apparently due to CD's adsorption on the liposomes and the formation of the defects in the bilayer. It is important to note that the highest release rate is characteristic of HPCD and AMCD. This is probably due to the fact that HPCD has the largest number of hydroxyl groups in its structure, and consequently, more hydrogen bonds are formed between the phosphate groups of lipids and −OH groups of HPCD. AMCD has a positively charged amino group (Table 1), so electrostatic interactions are expected between the charged $–NH_2$ of AMCD and negatively charged lipid heads. This is in good agreement with our previous research [31]; we demonstrated the interaction between PO_2^- groups of the lipids with -OH and $-NH_2$ groups on chitosan and chitosan-mannose conjugate by FTIR spectroscopy.

Thus, CD's adsorption on the liposomal membrane plays an important role for the formation of defects in the bilayer. According to the degree of occurrence of defects we have ranked CDs: AMCD >> HPCD > MCD ~ SBCD.

In case of CDpols (Figure 2.C), the release acceleration is 2 times higher than for CDs during first 60 minutes. Most likely, CDpol's particles have more functional groups for the interaction with the vesicles. Moreover, polymer particles might have a higher charge density that also affects the occurrence of defects. For instance, AMCD and AMCDpol have almost the same effect on membrane integrity due to the close ζ-potential values (Table 1).

Thus, CDpol causes two-times more defects in liposomal bilayer than CDs. Such effects can lead to the bacterial membrane damage and/or contribute to improving of drug penetration through biological barriers, therefore, increase its antibacterial activity.

3.3. Antibacterial activity of LV and its complexes with CD's derivatives

For *in vitro* studies we chose fluoroquinolone levofloxacin (LV) as a broad-spectrum antibacterial agent [32] that forms «guest»-«host» complexes with CD's carriers [33]. First, in order to discover the effectiveness of LV's incorporation into CD and CDpols in solid state we have obtained powder X-ray diffraction (PXRD) patterns (Figure 3) as a gold standard procedure described for CD complexes e.g. in [34]. The PXRD pattern of LV (navy blue line) corresponds to a crystalline LV (CCDC code: YUJNUM02 deposited on Cambridge Structural Database) [35]. The PXRD patterns for MCD (red) and MCDpol (green) are mainly of amorphous phase which is in a good agreement of previously published data [36]. When LV is complexed with both CD carriers, PXRD pattern changes significantly: degree of crystallinity measured at the integral intensities of the «halo» and crystalline peaks is around 20%. Previously we have observed this type of changes for HPCD complex with another fluoroquinolone moxifloxacin [6]. Thus, in the solid state the main part of LV is complexed with CD.

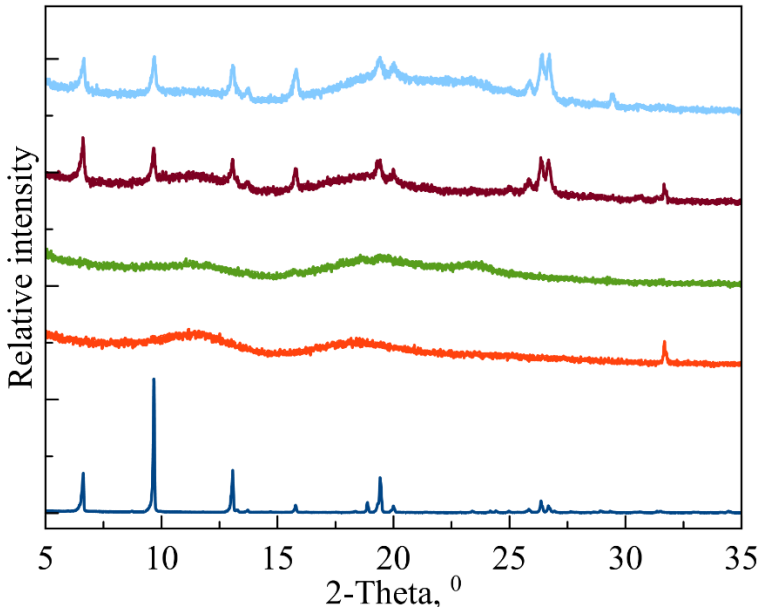

Figure 3. Experimental PXRD patterns for LV (navy blue), MCD (red) and MCDpol (green); LV-MCD (brown) and LV-MCDpol complexes (baby blue). From 35^{o} to 80^{o} no more signals were observed.

We investigated the effect of CD's carriers on LV's properties *in vitro* on five bacterial strains: gram-negative *Escherichia coli* MH1, *E.coli* JM109, *E. coli* ATCC 25922 and gram-positive *Lactobacillus fermentum* 90T-C4 and *Bacillus subtilis* ATCC 6633. It is known that gram-negative bacteria have outer lipid membrane, whereas gram-positive cells have peptidoglycan, so we expected especially pronounced effects on *E.coli* [37].

Agar well diffusion method was used to study antibacterial properties LV's formulations (Figure 4.A) as one of the most robust technics that allows to assess a set of drug's concentrations simultaneously [38,39].

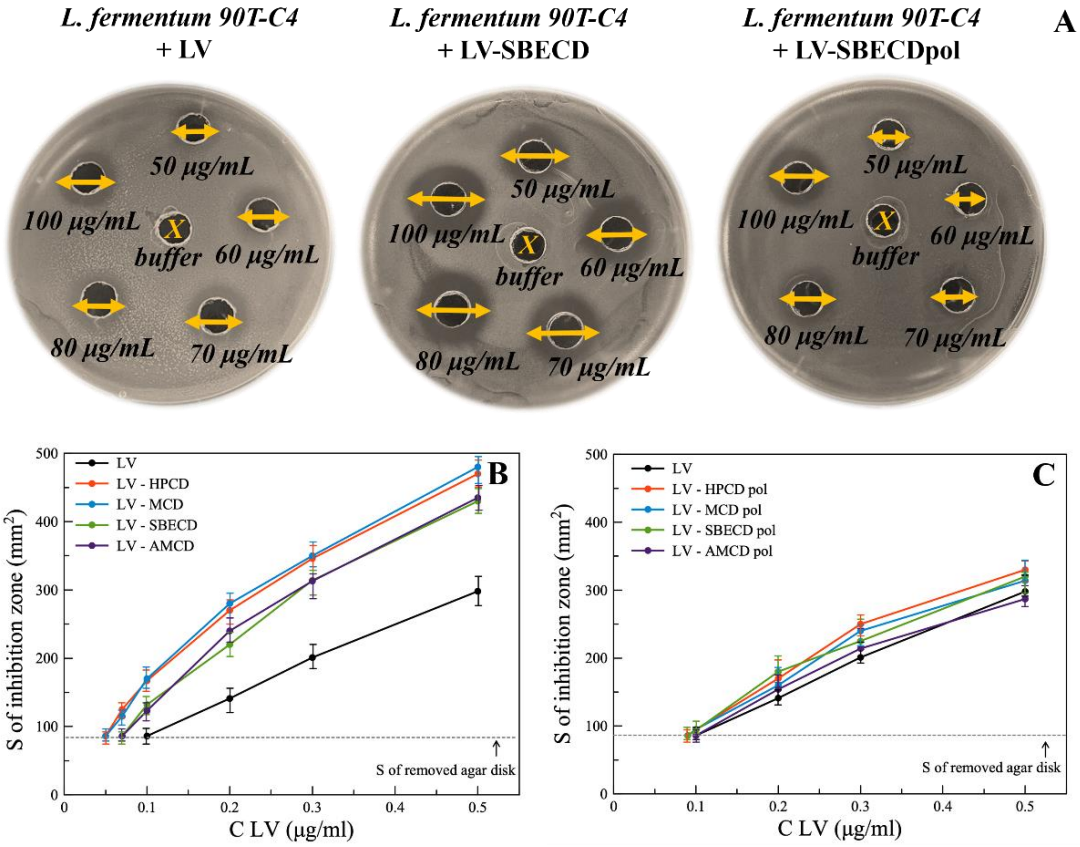

Figure 4. A. The diameters of inhibition zones (mm) on Petri dishes with free LV and its complexes with SBECD and SBECDpol in the concentration range 50–100 µg/mL, Agar well diffusion method, *L. fermentum* 90T-C4 pH 7.4 (0.02 M Na-phosphate buffer solution), 37°C, 24 h of incubation. B,C. The area of inhibition of *E. coli ATCC 25922* bacterial growths depending on the concentration of the drug, Agar well diffusion method, pH 7.4 (0.02 M Na-phosphate buffer solution), 37°C, 24 h of incubation.

Minimum inhibition concentration (MIC) was assumed as LV's concentration at which the inhibition area of bacteria equals the area of the removed agar disk. Table 2 represents MIC values for all bacterial strains.

MIC values differ significantly not only between bacterial species, but also within bacterial strains. Among *E. coli* strains the lowest MIC values 0.1 µg/mL is observed for *E. coli* MH1 and *E. coli* ATCC 25922 and the highest for *E. coli* JM109 (1 µg/mL). Higher resistance of *E. coli* JM109 might be associated with *gyrA96* mutation [20,40] that is the main target of LV [41]. For gram-positive bacteria $MIC_{L.\ fermentum\ 90T\text{-}C4}$ is more than 23 times higher than $MIC_{B.\ subtilis}$ which seems beneficial since lactobacilli are associated with probiotic properties [42].

All studied CDs and CDpols possess no antibacterial effect. This result is in good agreement with previous studies of these CD's derivatives [12,43]. Nevertheless, CD's substituent play a key role in CD's *in vitro* properties. In the study [44] the novel alkylamino CD's were synthesized that differ by the length and branching of terminal alkyl chain. The authors demonstrate CD's strong antibacterial activity depending on the number of carbon atoms in alkyl chain (from 4 to 7). The amino-CDs bearing alkyl groups consisting of 5-6 carbon atoms exhibit the highest antibacterial activity, equivalent to that of natural melittin (antibiotic peptide). If the number of carbon atoms is 4, then almost no effect is observed. These results are in good

agreement with our study, since we used the CD's derivatives with small terminal alkyl group (–CH_3 with one carbon atom) or terminal polar/charged groups.

Table 2. MIC values (μg/mL) for LV's formulations, Agar well diffusion method, pH 7.4 (0.02 M Na-phosphate buffer solution), 37°C, 24 h of incubation.

	E.coli **MH1**	***E.coli*** **JM109**	***E.coli*** **ATCC 25922**	***L. fermentum*** **90T-C4**	***B. subtilis*** **ATCC 6633**
LV	0.1 ± 0.02	1 ± 0.1	0.1 ± 0.02	45 ± 3	0.2 ± 0.03
MCD	-	-	-	-	-
AMCD	-	-	-	-	-
HPCDpol	-	-	-	-	-
MCDpol	-	-	-	-	-
LV-HPCD	0.12 ± 0.02	0.8±0.2	0.05 ± 0.01	22 ± 3	0.15 ± 0.02
LV-MCD	0.1 ± 0.02	0.8 ± 0.2	0.05 ± 0.01	22 ± 2	0.14 ± 0.01
LV-SBECD	0.08 ± 0.02	1 ± 0.1	0.07 ± 0.02	20 ± 2	0.15 ± 0.02
LV-AMCD	0.08 ± 0.02	1.1 ± 0.2	0.07 ± 0.02	25 ± 3	0.13 ± 0.03
LV-HPCDpol	0.1 ± 0.02	1 ± 0.1	0.1 ± 0.02	45 ± 3	0.18 ±0.02
LV-MCDpol	0.13 ± 0.02	1 ± 0.1	0.1 ± 0.02	45 ± 3	0.15 ± 0.02
LV-SBECDpol	0.1 ± 0.02	0.9 ± 0.1	0.1 ± 0.02	45 ± 2	0.13 ± 0.03
LV-AMCDpol	0.12 ± 0.02	1 ± 0.2	0.1 ± 0.02	36 ± 3	0.15 ± 0.03

LV-CD complexes demonstrate lower MIC values than free LV for both gram-positive and gram-negative cells. For *E. coli* MH1, *E. coli* JM109 and *B. subtilis* ATCC 6633 we observed only the slight or almost no CD's influence on LV's MIC. However, for *E. coli* ATCC 25922 and *L. fermentum* 90T-C4 CDs lowers MIC_{LV} dramatically (in almost 2 times). The increase of drug's action and decrease of it MIC was also observed for CD's complexes with essential oils (carvacrol and 2-Pentanoylfuran) [45]. This effect might be explained by the increase of drug's solubility, adsorption of LV-CD complexes on bacteria, the occurrence of membrane defects and/or facilitated LV's diffusion into the cells. Nevertheless, no specific influence of CD's substituent on the LV's activity was detected. All CDs demonstrate similar effect.

$MIC_{LV\text{-}CDpols}$ are close or slightly lower than MIC_{LV}. Less significant influence on LV's action for CDpols comparing to CD might be explained by the fact that large particles have limited diffusion through agar media, therefore, the antibacterial activity is comparable to the bacterial activity of LV.

Hence, the CDs and CDpols increase LV's antibacterial activity on gram-positive and gram-negative bacteria. For understanding the mechanism of such effect, we investigated the cells' state during LV-carrier exposure.

3.4. The influence of CDs and CDpols on bacteria's features

First, we studied the cells' composition by FTIR that is a powerful tool for differentiation and identification of bacteria. The FTIR spectra of cells (Figure 5) have a

number of distinctive peaks that are typical for all bacterial species [46]. The considerable region is 1300 − 900 cm^{-1} that contains signals from several cells' components, including DNA and phospholipids, as well as strong absorbance bands from complex sugar modes. Significant, intense bands within this region have been reported for different bacteria and assigned to the cell-wall components [47,48].

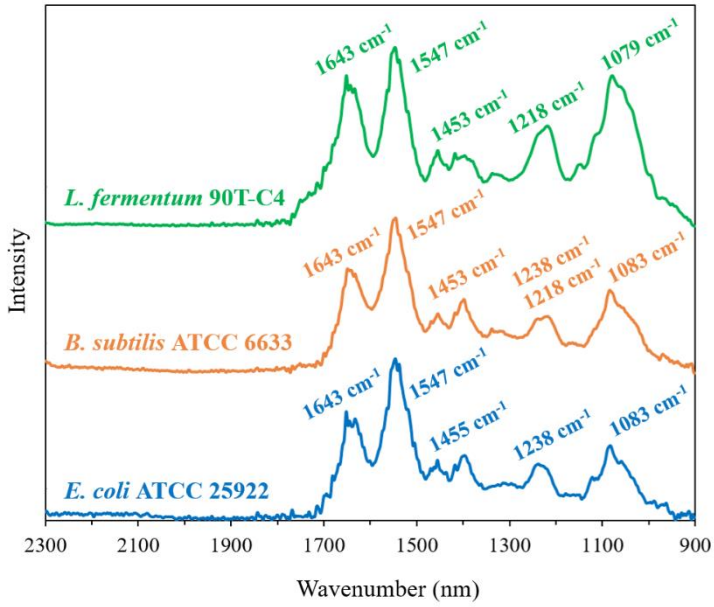

Figure 5. FTIR spectra of *L. fermentum* 90T-C4, *B. subtilis* ATCC6633 and *E. coli* ATCC 25922 in the range 2300 – 900 cm^{-1} of pure cultures of bacteria, ~ 10^{11} CFU/mL, H_2O, 22°C.

Three studied gram-negative *E.coli* strains demonstrate the same position and close intensity of the peaks. For *L. fermentum* 90T-C4 1218 cm^{-1} and 1079 cm^{-1} bands are remarkably intense comparing to *E.coli.* The finding was expected since these peaks are correlated with polysaccharides that are contained to a large extent in gram-positive bacteria's cell wall [46]. Interesting, that for gram-positive *B. subtilis* ATCC6633 and gram-negative *E.coli* we observed similar characteristics of its FTIR spectra that might be related to the special features of *B. subtilis.* Similar composition of *E.coli* and *B. subtilis* might lead to the close MIC values.

We have recently demonstrated that FTIR spectroscopy is a powerful tool to study the interaction between HPCD and liposomal membrane [18]. Briefly, HPCD caused the changes in the position of the bands, that corresponded to CH_2, PO_2^- and C=O groups in the FTIR spectra of liposomes. Thus, we expected to observe the changes in bacteria's FTIR spectra that can appear due to CD's administration: mainly 1300 − 900 cm^{-1} region that correspond to cell's surface. However, interactions of CDs or CDpols with bacteria did not lead to the changes in cells' spectra ($C_{CD\ torus}$ ~ 500 μg/mL). We suppose that, unlike liposomes, where lipids are more accessible for interaction with CD carriers, bacterial membrane have a number of proteins and the interaction is more complicated. Or the carriers might have mild effect on bacteria that can not be studied by FTIR spectroscopy, so we conducted the ultrastructural studies by transmission electron microscopy (TEM).

TEM is an efficient tool to examine the living, dead and dividing cells [12]. What is more interesting in our case, one can detect the changes in bacteria's structure and determine the mechanism of substance action. For instant, chitosan damages bacterial membrane [49]; peptide nisin causes partial cell-wall detachment from the plasma membrane [50] and leaking cell contents [51]; andrographolide derivative

leads to the formation of large cytoplasmic aggregates, cell elongation with abnormal cell septation, cytoplasmic disintegration, and finally cell lysis [52].

The control *B. subtilis* ATCC6633's ultrastructure demonstrates homogeneous bacteria state: all cells are in the same growth phase (Figure 6. A,E). On the micrographs of bacteria exposed by LV, LV–SBECD, or LV–SBECDpol for 24 hours (Figure 6. B-D, F-H) the total number of cells is lower than in the control culture. Bacteria demonstrates the morphological heterogeneity and many dead cells were detected, however the majority of the bacterial cells retained a typical structural feature.

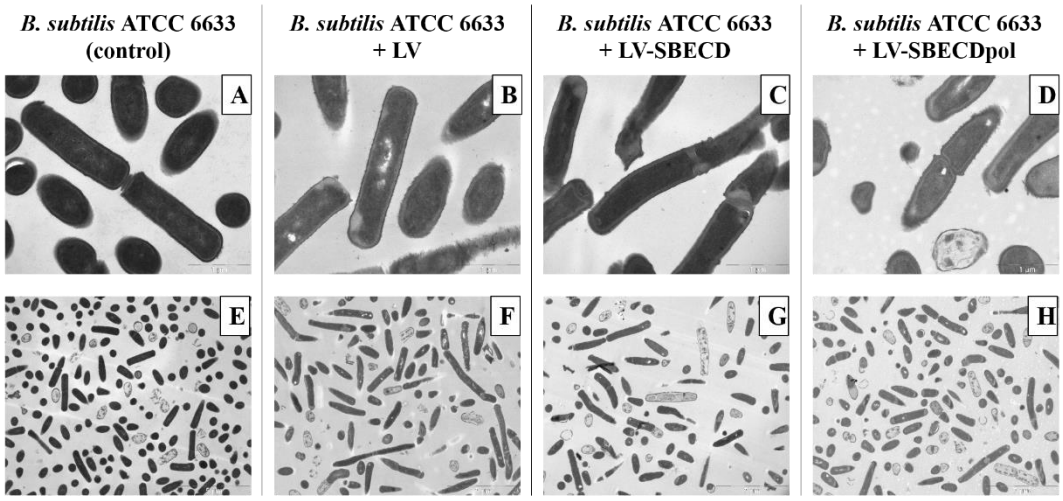

Figure 6. The TEM micrographs of *B. subtilis* ATCC6633: overnight culture, cells incubated with LV, LV-SBECD or LV-SBECDpol for 24 hours at 37 °C. C_{LV} = 2,5 μg/mL. Scale bar – 1 μm (A-D) and 5 μm (E-H).

Still, no specific effect of CD or CDpols on the morphology the cell wall, membrane or cytoplasm is detected that proves – CDs might only have a mild effect on the cell's membrane. The defects that may occur are not lethal for cells, so there must be other reasons for the 2-times increase of LV's activity *in vitro*. One of the main factor might be associated with carrier's adsorption on the bacteria surface resulting in a high local concentration of the drug.

3.4. Adsorption of LV-CDs and LV-CDpols on bacteria

As we have shown in previous section electrostatic interaction between the liposomal membrane and CD based carrier is one of the main factor of their interaction. Thus, we studied ζ-potential of the bacterial surface (Table 3).

Table 3. ζ-potential (mV) of bacterial cells, pH 7.4 (0.02 M Na-phosphate buffer solution), 22°C.

E.coli **MH1**	*E.coli* **JM109**	*E.coli* **ATCC 25922**	*L. fermentum* **90T-C4**	*B. subtilis* **ATCC 6633**
-36.8 ± 4.5	-35.5 ± 5.6	-34.7 ± 4.8	-11.2 ± 0.5	-23.1 ± 0.5

All bacteria possess pronounced negative ζ-potential that is in good agreement with literature data [37,53]. Gram-positive bacteria demonstrate higher charge than gram-negative, so we expected better LV-CDs and LV-CDpols adsorption on *L. fermentum* 90T-C4 and *B. subtilis* ATCC6633. Nevertheless, cells and liposomes have comparable ζ-potential values, and we expected to determine similar tendencies of

CD's interaction with the bacterial membrane, which were observed when studying CD-liposomes.

The adsorption curves are presented as the dependence of absorbed LV on the added LV's concentration (Figure 7). Comparing the slopes of linear curves, we found that for gram-negative strains the formation of LV–CD complexes leads to the increase of LV's absorption, whereas for gram-positive bacteria the opposite trend is observed. This unexpected result indicates the importance of bacterial membrane in the interaction with CD's carriers.

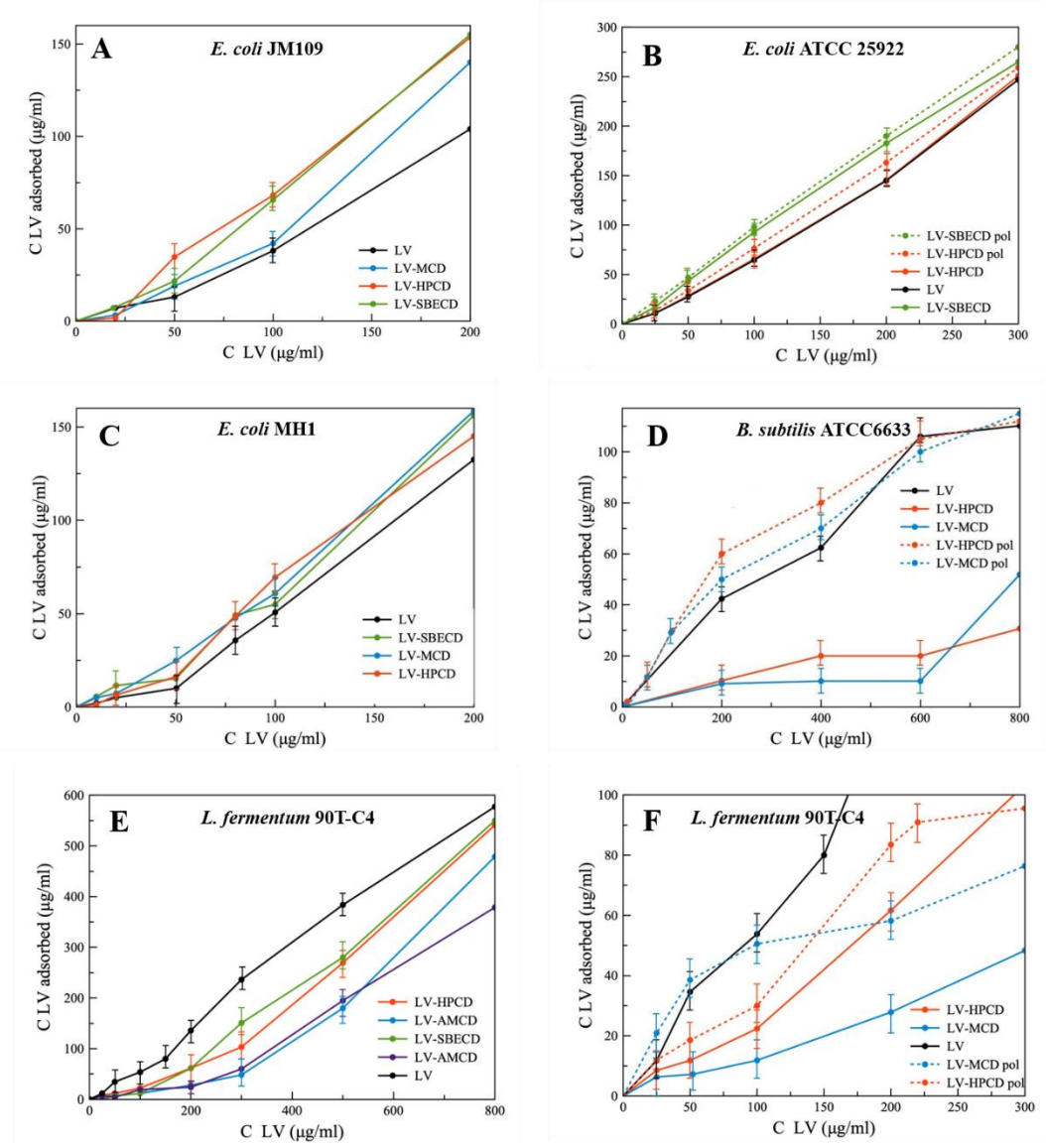

Figure 7. The absorption curves of LV, LV–CD and LV-CDpol on bacterial strains, ~ 1×10^9 cells/mL, pH 7.4 (0.02 M Na-phosphate buffer solution), 1 hour of incubation, 37°C.

On average among all LV-CD complexes, HPCD demonstrates the most pronounced increase of LV's adsorption on bacteria. As HPCD demonstrated high acceleration of PP's release from liposomes, we consider electrostatic interactions are not the main factor for CD's adsorption on bacterial cells. The mechanism of interaction between CDs and multi-component bacterial membrane must be studied in details.

For all bacterial strains LV-CDpols are adsorbed better than LV-CD, which confirms the results obtained during the experiment with PP's release from liposomes

(Figure 2). On average, polymers are adsorbed 15% more effectively for *E.coli*, in 2.3 times for lactobacilli and in 5 times for *B. subtilis*. That indicates LV-CDpols are more promising drug carriers than LV-CD.

The most significant effect on LV's adsorption is observed for HPCDpol and MCDpol that possess the highest ζ-potential (Table 1). So, for CDpols electrostatic interactions plays the key role of CDpol – cell's membrane interactions. We suppose multiple charged functional groups help CDpols to be retained at many binding sites on cells.

The differences between the morphology of bacteria surface might also influence LV-CDs and LV-CDpols adsorption, so we studied the bacteria surface by TEM.

3.5. The influence of bacterial cell's morphology on LV forms adsorption

The Figure 8 demonstrates TEM micrographs of bacterial strains. All gram-negative *E. coli* strains possess a number of long (approximately 5 μm) flagella, more than one for each cell. In addition, *E. coli* JM109's and *E.coli* ATCC 25922's surface is all covered with proteinaceous fimbria that are 300-1000 nm in length. Visually *E. coli* ATCC 25922 is characterized by more numerous fimbriae that are thinner and shorter compared to the *E. coli* JM109. Fimbria mainly help the bacteria to adhese and transfer genetic information [54] that might improve adhesion of LV's forms. Indeed, for *E. coli* JM109 and *E. coli* ATCC 25922 the adsorption is in almost 2 times higher than for *E. coli* MH1 (Table S1).

In contrast, gram-positive *L. fermentum* 90T-C4 do not have flagella or fimbriae. Cells' surface is smooth and homogeneous, while *E. coli* is characterized by a «rough» surface. The micrograph of lactobacilli also clearly shows the thick cell wall of peptidoglycan. *B. subtilis* ATCC6633 demonstrated low adhesion ability on the formvar-coated EM grids that might be due to lipophilic bacteria capsule. The micrographs uncovered only a numerous flagella (data not shown).

The smooth surface of gram-positive bacteria might be the reason for/cause of the lower adhesion on the cells, whereas the «rough» surface of gram-negative bacteria with fimbria increases the adhesion of both LV-CD and LV-CDpols demonstrated in previous section (Figure 7).

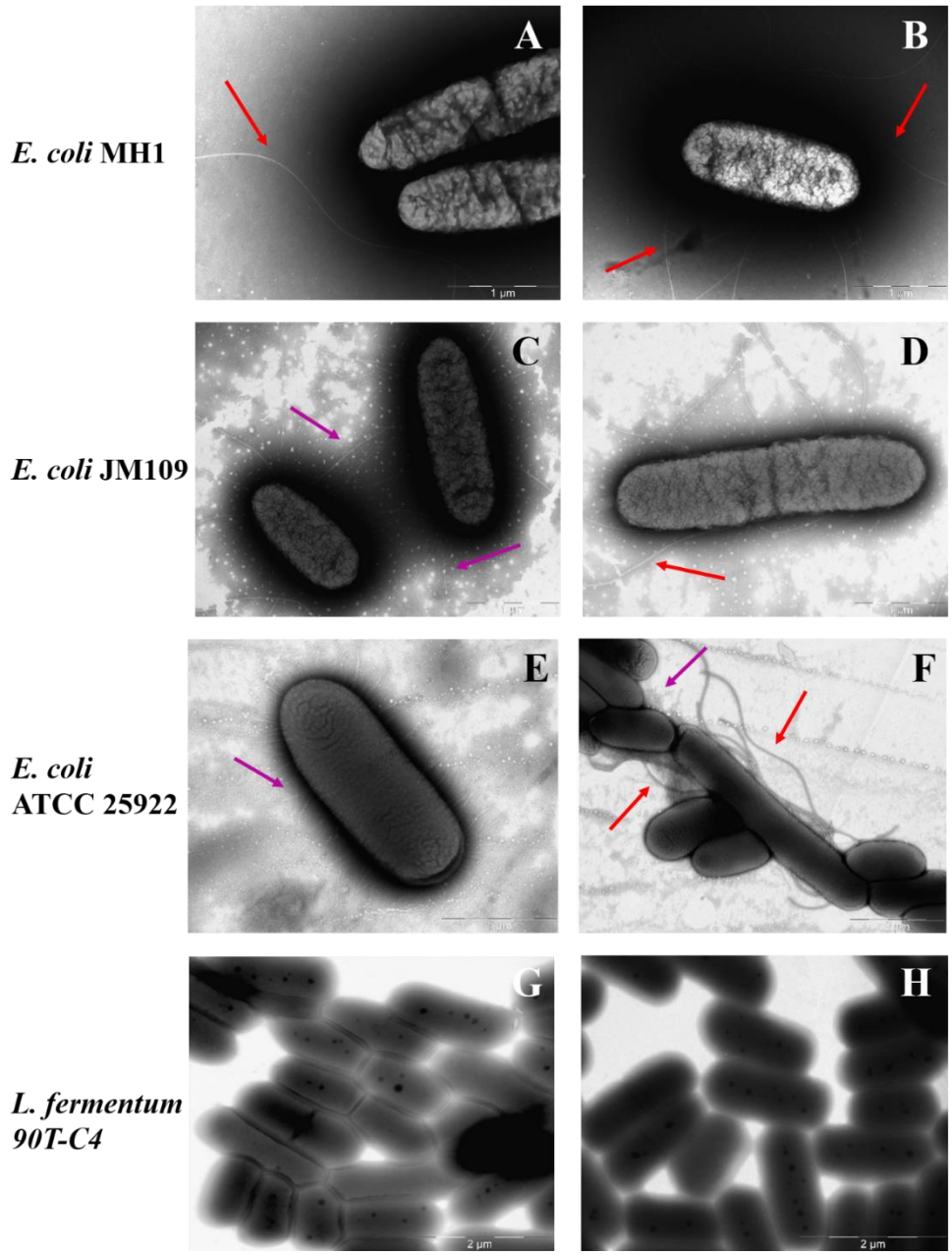

Figure 8. The morphology of bacterial surface: *E. coli* MH1 (A, B), *E.coli* JM109 (C, D), *E. coli* ATCC 25922 (E, F), *L. fermentum* 90T-C4 (G, H). Purple arrows indicate fimbria and red arrows are for flagella. Scale bars – 1 µm (A-E) and 2 µm (F-H).

3.5. Visualisation of CDpols adsorbtion on bacteria

To confirm the CDpols adsorption on bacterial cells we visualized the adhesion by TEM. Due to high solubility and a lack of the heavy atoms, CD's visualization by TEM is complicated. Some authors obtain metal complexes [55] or use the drug with aromatic core with additional contrast by sodium phosphotungstate [56]. We obtained HPCDpol-Cu^{2+} using copper (II) sulfate. However, even contrasted polymer was challenging to visualize.

In order to avoid desorption of particles from the cells' surface, no phosphotungstic acid was used. In such conditions, bacteria appear as black oval shapes with light grey areas. No flagella or fimbria are visible. Earlier Nadtochenko et al. demonstrated similar bacteria image [57].

It should be noted that cell's images vary significantly within bacterial species. We selected the most suitable copper (II) ions' concentration which do not lead to the observable changes of the bacteria' shape or cytoplasm. Figure 9 demonstrates particle's absorption on *B. subtilis* ATCC 6633 and *L. fermentum* 90T-C4.

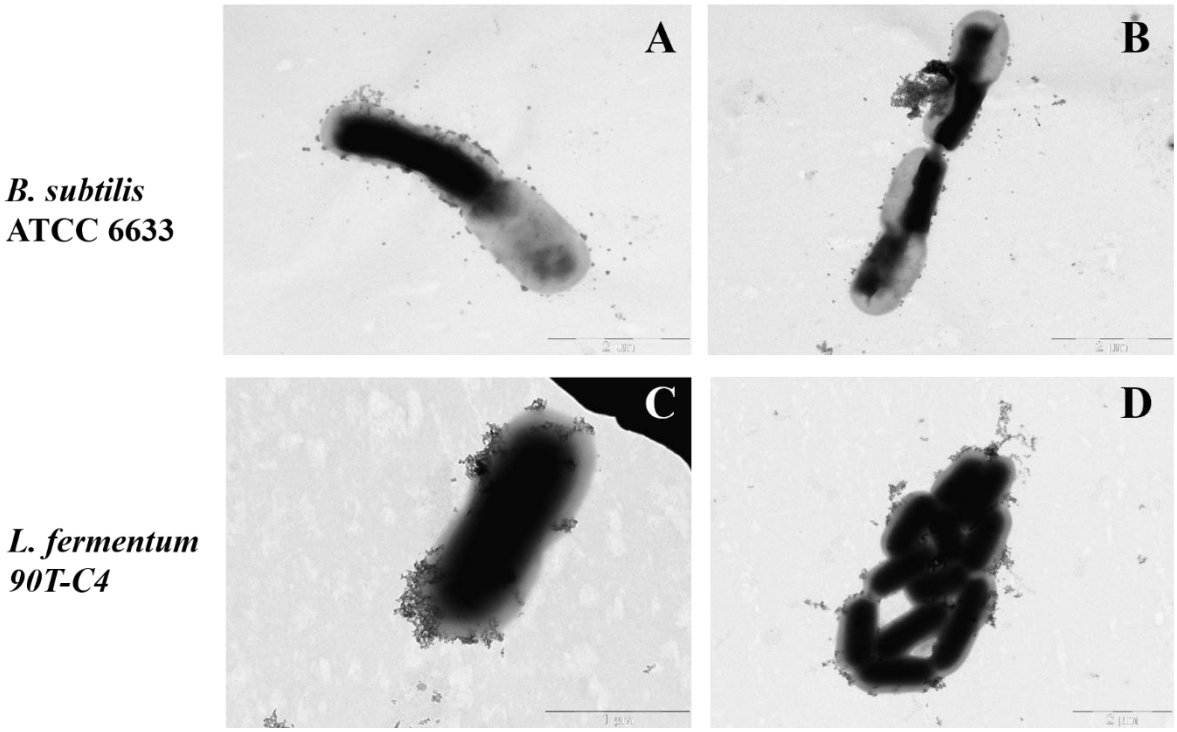

Figure 9. The TEM microphotographs of HPCDpol-Cu^{2+} particles adsorption on *B. subtilis* ATCC 6633 (A-B) and *L. fermentum* 90T-C4 (C–D), H_2O, 20 min of incubation, 37^{o}C, C(Cu^{2+}) ~ 0.001M, 80 mV. Scale bars – 1 μm (C) and 2 μm (A, B, D).

According to the results, HPCDpol-Cu^{2+} forms aggregates, but does not possess any selectivity to the bacterial surface: the particles distribute evenly over the cell's surface. No visible defects in bacterial surface or cell's shape are observed, that proves that CDpols have a mild effect on bacteria. Besides the defects in cell's surface, CD and CDpols adsorption on bacteria lead to high local concentration of LV that, in consequence, lowers MIC_{LV} in almost 2 times. Thus, the formation of CD-drug complexes is of great interest to develop drug formulation with increased antibacterial action.

4. Conclusions

Here, we studied the interaction of biomembranes (both liposomal and bacterial) with drug carriers CDs and CDpols that differ in size, mass and ζ-potential (Table 1). The crosslinking of CDs with 1.6-hexamethelenediisocyanate lead to the formation of the urethane nanoparticle with terminal charged NH_2 groups, which form due to the hydrolysis of isocyanine groups. We found that CD and CDpols adsorb on liposomal bilayer (DPPC / CL = 80 / 20 (weight %)) and cause the defects. Pronounced positive ζ-potential (> 10 mV), multiple -OH groups and nanoparticle structure increase the defects occurrence in 2 times. In case of bacterial membrane the interaction is more complicated.

PXRD experiments discovered that the main part of drug LV is complexed with the CD matrix. For LV-CD's adsorption on bacteria electrostatic interactions are not the main factor, whereas for LV- CDpols adsorption is associated with multiple electrostatic interactions between positively charged $-NH_2$ groups and many binding sites on cells' surface.

We demonstrate that the morphology of bacterial cell plays an important role in LV-carrier adhesion. The gram-positive bacteria with smooth surface adsorb less LV-carrier than gram-negative bacteria *E. coli* with «rough» surface and protein fimbria. Nevertheless, even without fimbria the outer membrane of the gram-negative bacteria prefers the absorbance of LV-CD than LV. Comparing LV-CDs and LV-CDpols, polymers are adsorbed 15% more for *E.coli*, in 2.3 times for lactobacilli and in 5 times for *B. subtilis*.

CD and CDpols lowers MIC_{LV} in almost 2 times. TEM approaches proves that CD carriers are not lethal for bacteria, but mild defects may occur that cannot be detected. We consider that CD and CDpols might extract lipids and/or proteins from bacterial surface that might cause mild damages in the membrane and, as a consequence, lead to the increase of LV's antibacterial action.

Supplementary Materials: The following supporting information can be downloaded at: www.mdpi.com/xxx/s1, Figure S1 (^{1}H NMR and FTIR spectra of MCD and MCDpol); Table S1 (The slopes of adsorption curves).

Author Contributions: Conceptualization, A.A.S., I.M.L-D. and E.V.K.; methodology, A.A.S., N.G.B.; formal analysis, A.A.S., T. Yu. K. and I.M.L-D.; investigation, A.A.S., A.S.T., S.A.G., N.T.L. and T.Yu.K.; writing—original draft preparation, A.A.S. and A.S.T.; writing—review and editing, E.V.K., I.M.L-D., A.S.T. and A.A.S.; supervision, E.V.K. and I.M.L-D. All authors have read and agreed to the published version of the manuscript.

Funding: This work was supported by Russian Science Foundation (grant number 22-24- 501 00604 (E.V.K. for CD's purchase)) and by Russian Foundation of Fundamental Research and Moscow Government (grant number 21-33-70035 (I.M.L-D., A.A.S.; for lipids' purchase)).

Data Availability Statement: Not applicable.

Acknowledgments: The work was performed using equipment (FTIR spectrometer Bruker Tensor 27 and Jasco J-815 CD Spectrometer) of the program for the development of Moscow State University and equipment purchased by the Developmental program of Lomonosov Moscow State University (PNR 5.13). The work was supported by Scholarship of the President of the Russian Federation for young scientists and postgraduates.

Conflicts of Interest: The authors declare no conflict of interest.

Abbreviations

The following abbreviations are used in this manuscript:

CD	Cyclodextrin
CDpol	Polymer based on cyclodextrin
HPCD	2-hydroxypropyl-β-cyclodextrin
MCD	Methyl-β-cyclodextrin
SBECD	Sulfobutyl ether β-cyclodextrin
AMCD	Amino-β-cyclodextrin
LV	Levofloxacin
CL	Cardiolipin
DPPC	Dipalmitoylphosphatidylcholine
PP	Phenolphthalein
MIC	Minimum inhibition concentration
CFU	Colony-forming units
FTIR	Fourier transform infrared spectroscopy

TEM	Transmission electron microscopes
UV	Ultraviolet spectroscopy
NTA	Nanoparticle data analysis
DLS	Dynamic light scattering
PXRD	Powder X-ray Diffraction

622

References

1. Dua, K.; Rapalli, V.K.; Shukla, S.D.; Singhvi, G.; Shastri, M.D.; Chellappan, D.K.; Satija, S.; Mehta, M.; Gulati, M.; Pinto, T.D.J.A.; et al. Multi-Drug Resistant Mycobacterium Tuberculosis & Oxidative Stress Complexity: Emerging Need for Novel Drug Delivery Approaches. *Biomed. Pharmacother.* **2018**, *107*, 1218–1229, doi:10.1016/j.biopha.2018.08.101.
2. Pons-Faudoa, F.P.; Ballerini, A.; Sakamoto, J.; Grattoni, A. Advanced Implantable Drug Delivery Technologies: Transforming the Clinical Landscape of Therapeutics for Chronic Diseases. *Biomed. Microdevices* **2019**, *21*, doi:10.1007/s10544-019-0389-6.
3. Jansook, P.; Ogawa, N.; Loftsson, T. Cyclodextrins: Structure, Physicochemical Properties and Pharmaceutical Applications. *Int. J. Pharm.* **2018**, *535*, 272–284, doi:10.1016/j.ijpharm.2017.11.018.
4. Řezanka, M. Synthesis of Substituted Cyclodextrins. *Environ. Chem. Lett.* **2019**, *17*, 49–63, doi:10.1007/s10311-018-0779-7.
5. Kicuntod, J.; Sangpheak, K.; Mueller, M.; Wolschann, P.; Viernstein, H.; Yanaka, S.; Kato, K.; Chavasiri, W.; Pongsawasdi, P.; Kungwan, N.; et al. Theoretical and Experimental Studies on Inclusion Complexes of Pinostrobin and β-Cyclodextrins. *Sci. Pharm.* **2018**, *86*, 1–15, doi:10.3390/scipharm86010005.
6. Le-Deygen, I.M.; Skuredina, A.A.; Uporov, I. V.; Kudryashova, E. V. Thermodynamics and Molecular Insight in Guest–Host Complexes of Fluoroquinolones with β-Cyclodextrin Derivatives, as Revealed by ATR-FTIR Spectroscopy and Molecular Modeling Experiments. *Anal. Bioanal. Chem.* **2017**, *409*, 6451–6462, doi:10.1007/s00216-017-0590-5.
7. Sali, N.; Csepregi, R.; Kőszegi, T.; Kunsági-Máté, S.; Szente, L.; Poór, M. Complex Formation of Flavonoids Fisetin and Geraldol with β-Cyclodextrins. *J. Lumin.* **2018**, *194*, 82–90, doi:10.1016/j.jlumin.2017.10.017.
8. Skuredina, A.A.; Kopnova, T.Y.; Le-deygen, I.M.; Kudryashova, E. V Physical and Chemical Properties of the Guest – Host Inclusion Complexes of Cyprofloxacin with β -Cyclodextrin Derivatives. *Moscow Univ. Chem. Bull.* **2020**, *75*, 218–224, doi:10.3103/S0027131420040069.
9. García-Padial, M.; Martínez-Ohárriz, M.C.; Isasi, J.R.; Zornoza, A. Sorption and Release of Natural Phenolic Antioxidants in Different Cyclodextrin Polymers. *J. Agric. Food Chem.* **2017**, *65*, 4905–4910, doi:10.1021/acs.jafc.7b01591.
10. Pellicer, J.A.; Rodríguez-López, M.I.; Fortea, M.I.; Gabaldón Hernández, J.A.; Lucas-Abellán, C.; Mercader-Ros, M.T.; Serrano-Martínez, A.; Núñez-Delicado, E.; Cosma, P.; Fini, P.; et al. Removing of Direct Red 83:1 Using α- and HP-α-CDs Polymerized with Epichlorohydrin: Kinetic and Equilibrium Studies. *Dye. Pigment.* **2018**, *149*, 736–746, doi:10.1016/j.dyepig.2017.11.032.
11. Anne, J.M.; Boon, Y.H.; Saad, B.; Miskam, M.; Yusoff, M.M.; Shahriman, M.S.; Zain, N.N.M.; Lim, V.; Raoov, M. β-Cyclodextrin Conjugated Bifunctional Isocyanate Linker Polymer for Enhanced Removal of 2,4-Dinitrophenol from Environmental Waters. *R. Soc. Open Sci.* **2018**, *5*, 1–22, doi:10.1098/rsos.180942.
12. Skuredina, A.A.; Tychinina, A.S.; Le-Deygen, I.M.; Golyshev, S.A.; Belogurova, N.G.; Kudryashova, E. V. The Formation of Quasi-Regular Polymeric Network of Cross-Linked Sulfobutyl Ether Derivative of β-Cyclodextrin Synthesized with Moxifloxacin as a Template. *React. Funct. Polym.* **2021**, *159*, 104811, doi:10.1016/j.reactfunctpolym.2021.104811.
13. Hemine, K.; Skwierawska, A.; Kernstein, A.; Kozłowska-Tylingo, K. Cyclodextrin Polymers as Efficient Adsorbents for Removing Toxic Non-Biodegradable Pimavanserin from Pharmaceutical Wastewaters. *Chemosphere* **2020**, *250*, 126250, doi:10.1016/j.chemosphere.2020.126250.
14. Trotta, F.; Caldera, F.; Cavalli, R.; Soster, M.; Riedo, C.; Biasizzo, M.; Uccello Barretta, G.; Balzano, F.; Brunella, V. Molecularly Imprinted Cyclodextrin Nanosponges for the Controlled Delivery of L-DOPA: Perspectives for the Treatment of Parkinson's Disease. *Expert Opin. Drug Deliv.* **2016**, *13*, 1671–1680, doi:10.1080/17425247.2017.1248398.
15. Moya-Ortega, M.D.; Alvarez-Lorenzo, C.; Sigurdsson, H.H.; Concheiro, A.; Loftsson, T. γ-Cyclodextrin Hydrogels and Semi-Interpenetrating Networks for Sustained Delivery of Dexamethasone. *Carbohydr. Polym.* **2010**, *80*, 900–907, doi:10.1016/j.carbpol.2010.01.004.

16. Skuredina, A.A.; Le-Deygen, I.M.; Kudryashova, E. V. The Effect of Molecular Architecture of Sulfobutyl Ether β-Cyclodextrin Nanoparticles on Physicochemical Properties of Complexes with Moxifloxacin. *Colloid J.* **2018**, *80*, 312–319, doi:10.1134/S1061933X18030134.
17. Challa, R.; Ahuja, A.; Ali, J.; Khar, R.K. Cyclodextrins in Drug Delivery: An Updated Review. *AAPS PharmSciTech* **2005**, *2*, 329–357, doi:10.1517/17425247.2.1.335.
18. Skuredina, A.A.; Tychinina, A.S.; Le-Deygen, I.M.; Belogurova, N.G.; Kudryashova, E. V Regulation of Properties of Lipid Membranes by Interaction with 2-Hydroxypropyl β-Cyclodextrin : Molecular Details. *Russ. J. Bioorganic Chem.* **2020**, *46*, 692–701, doi:10.1134/S1068162020050246.
19. Goddard, J.M.; Caput, D.; Williams, S.R.; Martin, D.M. Cloning of Human Purine-Nucleoside Phosphorylase CDNA Sequences by Complementation in Escherichia Coli. *Proc. Natl. Acad. Sci. USA* **1983**, *80*, 4281–4285.
20. Yanisch-Perron, C.; Vieira, J.; Messing, J. Improved Ml3 Phage Cloning Vectors and Host Strains: Nucleotide Sequences of the M13mp18 and PUC19 Vectors. *Gene* **1985**, *33*, 103–119.
21. Skuredina, A.; Le-Deygen, I.; Belogurova, N.; Kudryashova, E. Effect of Cross-Linking on the Inclusion Complex Formation of Derivatized β-Cyclodextrins with Small-Molecule Drug Moxifloxacin. *Carbohydr. Res.* **2020**, 108183, doi:10.1016/j.carres.2020.108183.
22. Deygen, I.M.; Kudryashova, E. V New Versatile Approach for Analysis of PEG Content in Conjugates and Complexes with Biomacromolecules Based on FTIR Spectroscopy. *Colloids Surfaces B Biointerfaces* **2016**, *141*, 36–43, doi:10.1016/j.colsurfb.2016.01.030.
23. Balouiri, M.; Sadiki, M.; Ibnsouda, S.K. Methods for in Vitro Evaluating Antimicrobial Activity: A Review. *J. Pharm. Anal.* **2016**, *6*, 71–79, doi:10.1016/j.jpha.2015.11.005.
24. Damanhouri, Z.A.; Alkreathy, H.M.; Ali, A.S.; Karim, S. The Potential Role of Fluoroquinolones in the Management of Covid-19 a Rapid Review. *J. Adv. Pharm. Educ. Res.* **2021**, *11*, 125–134, doi:10.51847/FE1IOIPTWD.
25. Appelbaum, P.C.; Hunter, P.A. The Fluoroquinolone Antibacterials: Past, Present and Future Perspectives. *Int. J. Antimicrob. Agents* **2000**, *16*, 5–15, doi:10.1016/S0924-8579(00)00192-8.
26. Del Valle, E.M.M. Cyclodextrins and Their Uses: A Review. *Process Biochem.* **2004**, *39*, 1033–1046, doi:10.1016/S0032-9592(03)00258-9.
27. Szejtli, J. Introduction and General Overview of Cyclodextrin Chemistry. *Chem. Rev.* **1998**, *98*, 1743–1754, doi:10.1021/cr970022c.
28. Yang, C.; Li, H.; Goh, S.H.; Li, J. Cationic Star Polymers Consisting of α-Cyclodextrin Core and Oligoethylenimine Arms as Nonviral Gene Delivery Vectors. *Biomaterials* **2007**, *28*, 3245–3254, doi:10.1016/j.biomaterials.2007.03.033.
29. Du, X.; Song, N.; Yang, Y.W.; Wu, G.; Ma, J.; Gao, H. Reverse Micelles Based on β-Cyclodextrin-Incorporated Amphiphilic Polyurethane Copolymers for Protein Delivery. *Polym. Chem.* **2014**, *5*, 5300–5309, doi:10.1039/c4py00278d.
30. Hammoud, Z.; Khreich, N.; Auezova, L.; Fourmentin, S.; Elaissari, A.; Greige-Gerges, H. Cyclodextrin-Membrane Interaction in Drug Delivery and Membrane Structure Maintenance. *Int. J. Pharm.* **2019**, *564*, 59–76, doi:10.1016/j.ijpharm.2019.03.063.
31. Le-Deygen, I.M.; Rokosovina, V. V; Skuredina, A.A.; Yakimov, I.D.; Kudryashova, E. V The Charge and Phase State of Liposomes Dramatically Affects the Binding of Mannosylated Chitosan. *Futur. Pharmacol.* **2022**, *2*, 330–346, doi:10.3390/futurepharmacol2030023.
32. Liu, H.H. Safety Profile of the Fluoroquinolones: Focus on Levofloxacin. *Drug Saf.* **2010**, *33*, 353–369, doi:10.2165/11536360-000000000-00000.
33. Deygen, I.M.; Egorov, A.M.; Kudryashova, E. V. Structure and Stability of Fluoroquinolone-(2-Hydroxypropyl)-β-Cyclodextrin Complexes as Perspective Antituberculosis Drugs. *Moscow Univ. Chem.*

Bull. **2016**, *71*, 1–6, doi:10.3103/S0027131416010028.

34. Sala, A.; Hoossen, Z.; Bacchi, A.; Caira, M.R. Two Crystal Forms of a Hydrated 2:1 β-Cyclodextrin Fluconazole Complex: Single Crystal X-Ray Structures, Dehydration Profiles, and Conditions for Their Individual Isolation. *Molecules* **2021**, *26*, 1–14.
35. Freitas, J.T.J.; De Melo, C.C.; Viana, O.M.M.S.; Ferreira, F.F.; Doriguetto, A.C. Crystal Structure of Levofloxacin Anhydrates: A High-Temperature Powder X-Ray Diffraction Study Versus Crystal Structure Prediction. *Cryst. Growth Des.* **2018**, *18*, 3558–3568, doi:10.1021/acs.cgd.8b00363.
36. Kohut, A.; Demchuk, Z.; Kingsley, K.; Voronov, S.; Voronov, A. Dual Role of Methyl-β-Cyclodextrin in the Emulsion Polymerization of Highly Hydrophobic Plant Oil-Based Monomers with Various Unsaturations. *Eur. Polym. J.* **2018**, *108*, 322–328, doi:10.1016/j.eurpolymj.2018.09.010.
37. Seltmann, G.; Holst, O. *Cell Wall Models. In: The Bacterial Cell Wall.*; Springer, Berlin, Heidelberg, 2002;
38. Azhdarzadeh, M.; Lotfipour, F.; Zakeri-Milani, P.; Mohammadi, G.; Valizadeh, H. Anti-Bacterial Performance of Azithromycin Nanoparticles as Colloidal Drug Delivery System against Different Gram-Negative and Gram-Positive Bacteria. *Adv. Pharm. Bull.* **2012**, *2*, 17–24, doi:10.5681/apb.2012.003.
39. Valizadeh, H.; Mohammadi, G.; Ehyaei, R.; Milani, M.; Azhdarzadeh, M.; Zakeri-Milani, P.; Lotfipour, F. Antibacterial Activity of Clarithromycin Loaded PLGA Nanoparticles. *Pharmazie* **2012**, *67*, 63–68, doi:10.1691/ph.2012.1052.
40. Kuriki, Y. Temperature-Sensitive Amber Suppression of OmpF ' - ' LacZ Fused Gene Expression in a SupE Mutant of Escherichia Coli K12. **1993**, *107*, 71–76.
41. Blower, T.R.; Williamson, B.H.; Kerns, R.J.; Berger, J.M. Crystal Structure and Stability of Gyrase–Fluoroquinolone Cleaved Complexes from *Mycobacterium Tuberculosis*. *Proc. Natl. Acad. Sci.* **2016**, *113*, 1706–1713, doi:10.1073/pnas.1525047113.
42. Lee, C.S.; Kim, S.H. Anti-Inflammatory and Anti-Osteoporotic Potential of Lactobacillus Plantarum A41 and L. Fermentum SRK414 as Probiotics. *Probiotics Antimicrob. Proteins* **2020**, *12*, 623–634, doi:10.1007/s12602-019-09577-y.
43. Jug, M.; Kosalec, I.; Maestrelli, F.; Mura, P. Analysis of Triclosan Inclusion Complexes with β-Cyclodextrin and Its Water-Soluble Polymeric Derivative. *J. Pharm. Biomed. Anal.* **2011**, *54*, 1030–1039, doi:10.1016/j.jpba.2010.12.009.
44. Yamamura, H.; Hagiwara, T.; Hayashi, Y.; Osawa, K.; Kato, H.; Katsu, T.; Masuda, K.; Sumino, A.; Yamashita, H.; Jinno, R.; et al. Antibacterial Activity of Membrane-Permeabilizing Bactericidal Cyclodextrin Derivatives. *ACS Omega* **2021**, *6*, 31831–31842, doi:10.1021/acsomega.1c04541.
45. Liang, H.; Yuan, Q.; Vriesekoop, F.; Lv, F. Effects of Cyclodextrins on the Antimicrobial Activity of Plant-Derived Essential Oil Compounds. *Food Chem.* **2012**, *135*, 1020–1027, doi:10.1016/j.foodchem.2012.05.054.
46. Kochan, K.; Perez-Guaita, D.; Pissang, J.; Jiang, J.H.; Peleg, A.Y.; McNaughton, D.; Heraud, P.; Wood, B.R. In Vivo Atomic Force Microscopy-Infrared Spectroscopy of Bacteria. *J. R. Soc. Interface* **2018**, *15*, doi:10.1098/rsif.2018.0115.
47. Helm, D.; Labischinski, H.; Naumann, D. Elaboration of a Procedure for Identification of Bacteria Using Fourier-Transform IR Spectral Libraries: A Stepwise Correlation Approach. *J. Microbiol. Methods* **1991**, *14*, 127–142, doi:10.1016/0167-7012(91)90042-O.
48. Naumann, D.; Fijala, V.; Labischinski, H.; Giesbrecht, P. The Rapid Differentiation and Identification of Pathogenic Bacteria Using Fourier Transform Infrared Spectroscopic and Multivariate Statistical Analysis. *J. Mol. Struct.* **1988**, *174*, 165–170, doi:10.1016/0022-2860(88)80152-2.
49. Liu, H.; Du, Y.; Wang, X.; Sun, L. Chitosan Kills Bacteria through Cell Membrane Damage. *Int. J. Food Microbiol.* **2004**, *95*, 147–155, doi:10.1016/j.ijfoodmicro.2004.01.022.
50. Hyde, A.J.; Parisot, J.; McNichol, A.; Bonev, B.B. Nisin-Induced Changes in Bacillus Morphology Suggest a Paradigm of Antibiotic Action. *Proc. Natl. Acad. Sci. U. S. A.* **2006**, *103*, 19896–19901, doi:10.1073/pnas.0608373104.
51. Liu, H.; Pei, H.; Han, Z.; Feng, G.; Li, D. The Antimicrobial Effects and Synergistic Antibacterial Mechanism of the

Combination of ε-Polylysine and Nisin against Bacillus Subtilis. *Food Control* **2015**, *47*, 444–450, doi:10.1016/j.foodcont.2014.07.050.

52. Aromdee, C.; Sriubolmas, N.; Wiyakrutta, S.; Suebsasna, S.; Khunkitti, W. Effect of the Derivatives of Andrographolide on the Morphology of Bacillus Subtilis. *Arch. Pharm. Res.* **2011**, *34*, 71–77, doi:10.1007/s12272-011-0108-1.
53. Otto, K.; Elwing, H.; Hermansson, M. The Role of Type 1 Fimbriae in Adhesion of Escherichia Coli to Hydrophilic and Hydrophobic Surfaces. *Colloids Surfaces B Biointerfaces* **1999**, *15*, 99–111, doi:10.1016/S0927-7765(99)00050-8.
54. Proft, T.; Baker, E.N. Pili in Gram-Negative and Gram-Positive Bacteria - Structure, Assembly and Their Role in Disease. *Cell. Mol. Life Sci.* **2009**, *66*, 613–635, doi:10.1007/s00018-008-8477-4.
55. Pande, S.; Ghosh, S.K.; Praharaj, S.; Panigrahi, S.; Basu, S.; Jana, S.; Pal, A.; Tsukuda, T.; Pal, T. Synthesis of Normal and Inverted Gold-Silver Core-Shell Architectures in β-Cyclodextrin and Their Applications in SERS. *J. Phys. Chem. C* **2007**, *111*, 10806–10813, doi:10.1021/jp0702393.
56. Li, J.; Yang, M.; Xu, W.R. Enhanced Oral Bioavailability of Fluvastatin by Using Nanosuspensions Containing Cyclodextrin. *Drug Des. Devel. Ther.* **2018**, *12*, 3491–3499, doi:10.2147/DDDT.S177316.
57. Nadtochenko, V.A.; Rincon, A.G.; Stanca, S.E.; Kiwi, J. Dynamics of E. Coli Membrane Cell Peroxidation during TiO2 Photocatalysis Studied by ATR-FTIR Spectroscopy and AFM Microscopy. *J. Photochem. Photobiol. A Chem.* **2005**, *169*, 131–137, doi:10.1016/j.jphotochem.2004.06.011.